The structure of ice Ih from analysis of single-crystal neutron diffuse scattering

1995 J. Phys.: Condens. Matter 7 8259

(http://iopscience.iop.org/0953-8984/7/43/006)

J. Phys.: Condens. Matter 7 (1995) 8259–8271. Printed in the UK

The structure of ice Ih from analysis of single-crystal neutron diffuse scattering

V M Nield† and R W Whitworth

School of Physics and Space Research, University of Birmingham, Edgbaston, Birmingham B15 2TT, UK

Received 1 March 1995

Abstract. It has long been known that the single-crystal diffuse scattering from ice Ih contains a great deal of information about the hydrogen disorder and the local structure. A reverse Monte Carlo technique has been used to model such data from D_2O ice, and to explore the information which can be obtained about the structure of ice using it, most of which cannot be accessed using standard crystallographic techniques. As well as obtaining details of the average properties of the structure, the local disorder is obtained directly. While further developments are required for reverse Monte Carlo analysis of single-crystal diffuse scattering to produce highly accurate results, those presented here represent a leap forward in our analysis of the structure of ice from its diffuse scattering alone.

1. Introduction

The structure of ice Ih, the normal form of ice, has been extensively explored ever since the pioneering work of Bragg (1922) and it has long been known that the oxygen atoms occupy a regular tetrahedral network. However, the hydrogen atoms are disordered over four possible sites around each oxygen. The Bernal–Fowler rules (Bernal and Fowler 1933) require two of these sites to be occupied, with only one hydrogen between neighbouring oxygens. Hence each oxygen is involved in two covalent and two hydrogen bonds. Crystallographic studies (for example Peterson and Levy 1957, Kuhs and Lehmann 1986) have confirmed that whilst the Bernal–Fowler rules are obeyed the hydrogen atoms are otherwise disordered. It is this hydrogen disorder which makes it so difficult to obtain detailed information about the ice structure.

Analysis of the Bragg scattering from ice provides information on the average structure—the so-called half-hydrogen structure—in which each of the four hydrogen sites around an oxygen has half the scattering length of hydrogen in the neutron case, or half the hydrogen form factor for the case of x-rays. Hence, without additional information or assumptions, all that can be obtained are average quantities consistent with the tetrahedral site symmetry. Small static displacements related to the local disorder are impossible to differentiate from unusually large thermal vibrations.

It was realized that the single crystal diffuse scattering might provide additional information on the structure of ice Ih. Measurements and calculations of the scattering predicted by the Bernal–Fowler rules were made by several groups (Owston 1949, Axe and Hamilton, in Kamb 1973, Villain and Schneider 1973, Schneider 1975, Schneider and Just

† Present address: Physics Laboratory, University of Kent, Canterbury, Kent CT2 7NR, UK.

0953-8984/95/438259+13$19.50

1975, Schneider and Zeyen 1980, Descamps and Coulon 1977, Goto *et al* 1992) and were in reasonable agreement, providing further validation for a model with the Bernal–Fowler rules obeyed and the hydrogen atoms otherwise disordered. (In fact most such experiments were performed with neutrons and so with D_2O ice, because of the difficulty in separating the diffuse scattering from the large incoherent contribution of the H in H_2O ice.) There were significant differences between the experimental and calculated scattering in some regions of reciprocal space, however. This is discussed further in the next section and in Li *et al* (1994).

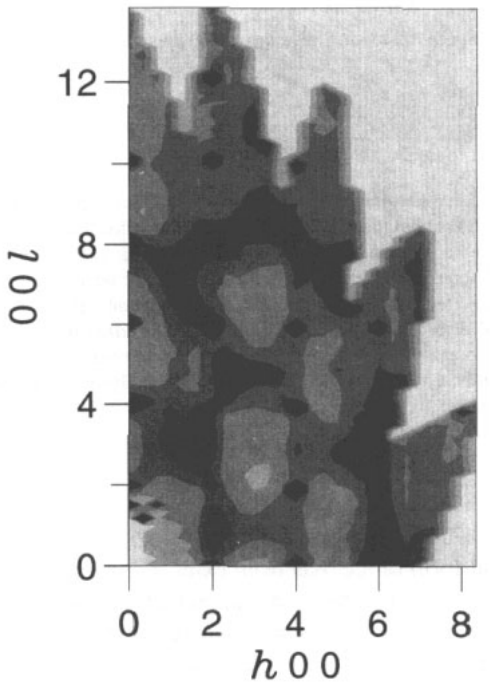

Figure 1. Experimental neutron scattering pattern in the $h\ 0\ l$ plane from D_2O ice Ih at 20 K. Darker shading corresponds to higher contour levels, which are the same in figures 1–5.

To increase our understanding of the diffuse scattering from ice a reverse Monte Carlo modelling technique (RMCX, described in detail in Nield *et al* 1995) has been applied. The information obtained on the structure of ice is discussed critically with reference to the present limitations of the modelling technique.

2. Experiment and Bernal–Fowler modelling

The single-crystal neutron diffuse scattering data used in this study was measured by J-C Li (Li *et al* 1994) on the single-crystal diffractometer, SXD, at the ISIS pulsed neutron source (Rutherford Appleton Laboratory, UK). Three different samples were used, each of approximately 1 cm in diameter and 1.5 cm effective height and all cut from the same large crystal of D_2O ice. Their orientations were such that one of the $h\ 0\ l$, $0\ k\ l$ and $h\ k\ 0$ planes (in orthorhombic notation) scattered into the equatorial plane of the detector in each case (these are the hexagonal $h\ h\ l$, $h\ 0\ l$ and $h\ k\ 0$ planes respectively). The samples were in turn placed in a standard cryostat and cooled to 20 K. The scattering over a large volume

of reciprocal space was measured, and the raw data corrected, absolutely normalized and converted to reciprocal lattice units (as described in Nield 1995). The resulting diffuse scattering in the $h\ 0\ l$ and $0\ k\ l$ planes is shown in figures 1 and 2 respectively.

The scattering from D_2O ice in which the deuterons are disordered but obey the Bernal–Fowler rules was calculated to compare with experiment, using the definition of the neutron scattering cross-section in the static approximation (Li *et al* 1994), which reduces to

$$F(\boldsymbol{Q}) = \frac{1}{2\pi N}\left|\sum_{i=1}^{N} \overline{b_i} \exp(\mathrm{i}\boldsymbol{Q}\cdot\boldsymbol{R}_i)\right|^2 \tag{1}$$

when the calculation is performed at $\boldsymbol{Q}$ points which satisfy

$$\boldsymbol{Q} = 2\pi\left(\frac{h'}{an_a}, \frac{k'}{bn_b}, \frac{l'}{cn_c}\right) \tag{2}$$

for lattice parameters a, b, c, and a configuration box of N atoms with n_a, n_b, n_c unit cells in the three directions. h', k', l' are integers. $F(\boldsymbol{Q})$ is the coherent part of the structure factor with $\boldsymbol{Q}$ the wave vector transfer and $\overline{b_i}$ the scattering length of atom i which is at position $\boldsymbol{R}_i$. From equation (2) $F(\boldsymbol{Q})$ can only be calculated on a grid of points in reciprocal lattice space, with the grid spacings inversely proportional to the number of unit cells, and so the data must be binned in accordance with this. In the present case the configuration consisted of $6 \times 6 \times 6$ eight-molecule orthorhombic unit cells. (The configuration is sometimes described as a super-cell, in which case the calculation is being performed at the Bragg peaks of that super-cell.)

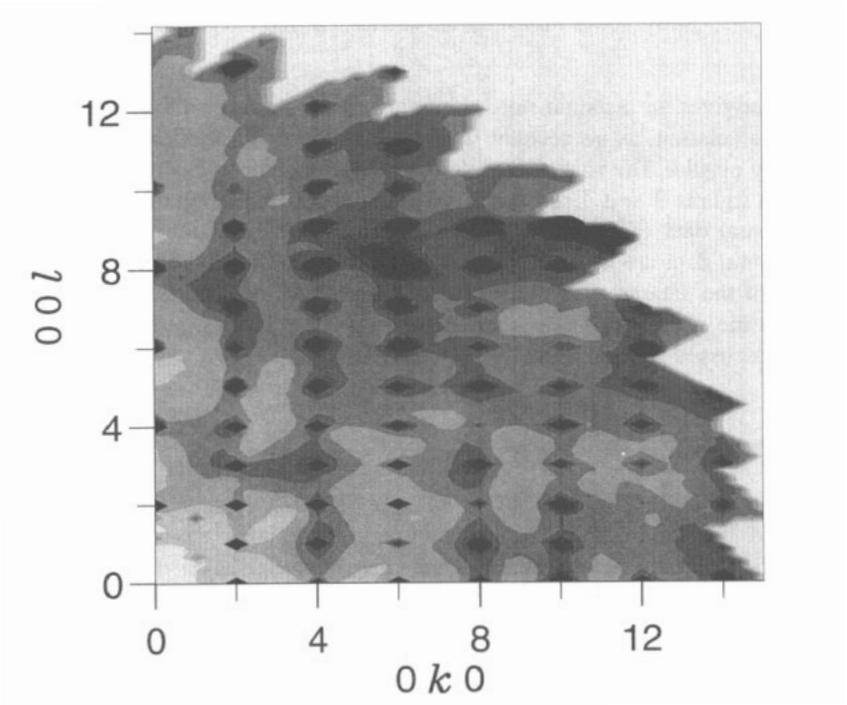

Figure 2. Experimental neutron scattering pattern in the $0\ k\ l$ plane from D_2O ice Ih at 20 K.

Equation (1) is derived from an expression involving an integral over all energies, and hence allows calculation of the total scattering, rather than the elastic scattering. The

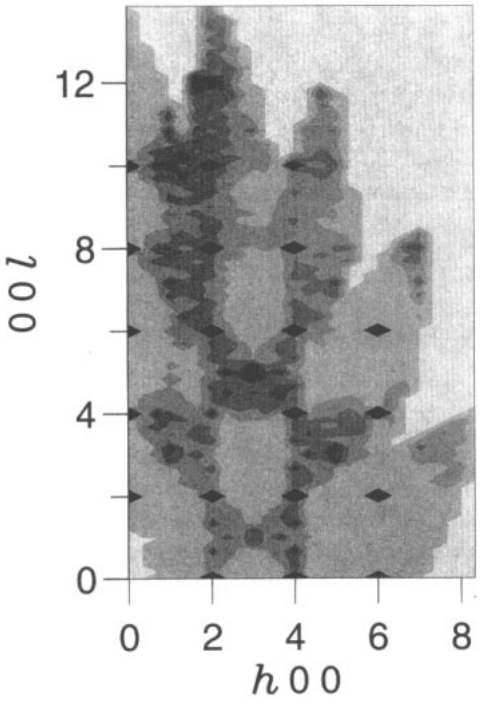

Figure 3. Predicted neutron scattering pattern in the $h\ 0\ l$ plane from D_2O ice in obeying the Bernal–Fowler rules. Compare with the scattering in figure 1.

expression gives an instantaneous picture, or 'snap-shot', of the structure. However, in the present calculation, as no account was taken of thermal vibration, the calculated scattering is entirely elastic. The scattering calculated in this manner for the $h\ 0\ l$ and $0\ k\ l$ planes is shown in figures 3 and 4 respectively, which should be compared with the corresponding experimental data of figures 1 and 2. It can be seen that the underlying features in the experimental data are those predicted by the simulation. However, not all of the dominant features of the data are reproduced by the simulation; in particular the streak along $6\ 0\ l$ is absent in the simulation, as is the patch of strong scattering at high Q in the $0\ k\ l$ plane. This is discussed in more detail in Li *et al* (1994).

3. Reverse Monte Carlo modelling

The reverse Monte Carlo (RMC) technique (McGreevy and Pusztai 1988) was initially developed for the interpretation of neutron diffraction data for liquids and amorphous materials. However, its applications are now numerous, and it can be used to model x-ray, neutron and EXAFS data, simultaneously or separately, from a very wide range of materials (McGreevy and Howe 1992). For the present work the RMC technique was extended to allow the simultaneous modelling of many planes of single crystal neutron diffuse scattering, as described in Nield *et al* (1995). This version of RMC is known as RMCX. No Bragg scattering was modelled in the present study.

In essence RMC is very simple, with the aim being to find a configuration of atoms which reproduces the experimental data. This is done using a Markov chain procedure. The technique is very similar to the better known Metropolis Monte Carlo method (Metropolis

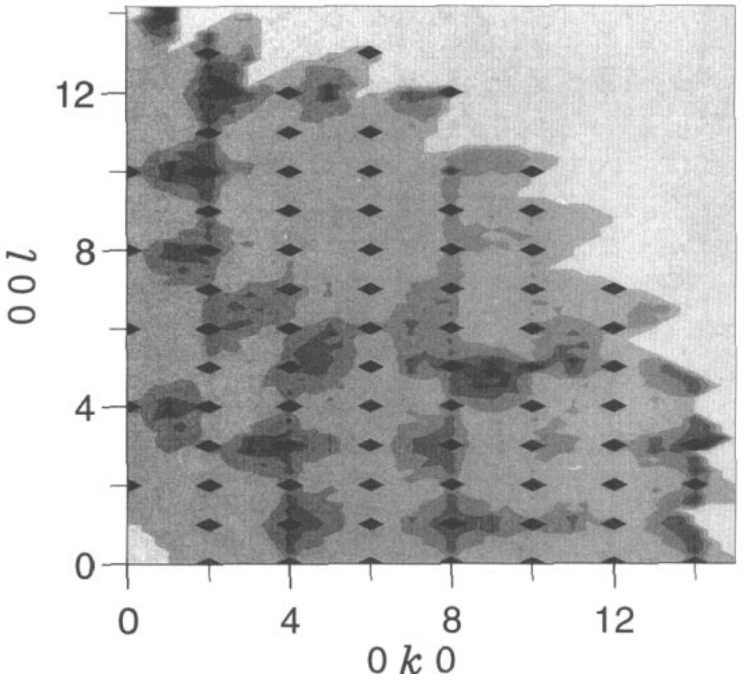

Figure 4. Predicted neutron scattering pattern in the 0 k l plane from D_2O ice Ih obeying the Bernal–Fowler rules. Compare with the scattering in figure 2.

et al 1953), in which the total energy of a configuration of atoms is minimized. In RMC no potential function is needed, and the difference between the experimental data and the same quantity calculated from the configuration of atoms is minimized.

The starting point in the present calculations was the end point from the Bernal–Fowler modelling discussed previously. Hence there were $6\times6\times6$ eight molecule orthorhombic unit cells (chosen to facilitate the use of periodic boundary conditions), with lattice constants $a = 4.498$ Å, $c = 7.323$ Å and $b = 2a\sin 60°$ because of the underlying hexagonal symmetry (Röttger *et al* 1994). The oxygen atoms were arranged so that all the O–O–O angles were tetrahedral (i.e. 109.47°) with the deuterons disordered whilst obeying the Bernal–Fowler rules. In the RMCX calculation an atom, either oxygen or deuteron, is chosen at random and moved a random amount, up to a user specified maximum, in a random direction. Periodic boundary conditions are applied. It is checked that the moved atom is not unphysically close to any other. The closest approach distances were taken as 2.3, 0.5 and 1.0 Å for O–O, O–D and D–D respectively.

In the present study five planes of diffuse scattering were modelled simultaneously. These were the orthorhombic h 0 l, and its equivalent the h 3h l; the 0 k l and its equivalent the h h l; and the h k 0. The two equivalent planes were included to try and enforce the hexagonal symmetry lost by modelling in an orthorhombic coordinate system. Twenty configurations were obtained, to provide adequate statistics for analysis, each taking 36 h of cpu time on a Digital VAX 4000/60. Figure 5 shows the fit to the h 0 l plane (averaged over the 20 configurations). Equally good fits were obtained to all planes of data.

It needs to be borne in mind that RMCX can often fit the data with which it is presented in many ways. This is especially true when the data quality decreases. In the present case the statistical accuracy of the data is not high and there are difficulties in accurate data

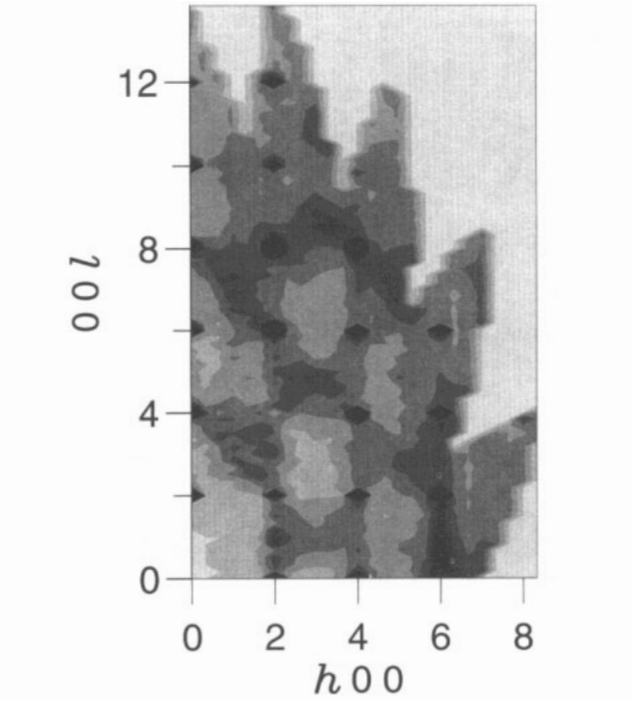

Figure 5. RMCX fit to the scattering of figure 1.

correction, because of the light deuterium atoms. The accuracy of the data is further decreased because some hydrogen contamination is inevitable. (The initial water purity was 99.9%, but handling is likely to have decreased this slightly.) Hydrogen gives very strong incoherent scattering and no attempt was made to separate any such component from the diffuse scattering. An additional calculation was carried out in which RMCX modelling was performed in exactly the manner just discussed, but with the oxygen atoms fixed to their sites. This was to allow some assessment of the accuracy of the results from the first model.

Limitations of the present RMCX technique are discussed in detail in section 5. To overcome some of the modelling problems tests are being performed in which Bragg and diffuse scattering from single crystals are modelled together using reverse Monte Carlo algorithms. This should improve the obtained values of mean square displacements and so on. However, at present this simultaneous modelling is impossible to apply to the present case, because of the prohibitive cpu time required (more than 10 times that used at present).

4. Analysis and notation

Each of the final configurations is an instantaneous 'snap-shot' structure, which is consistent with the experimental data. It is not the only structure which agrees with the data, but is hopefully a representative one. There are two completely different ways of obtaining information from the RMCX configuration, and these give two complementary pictures of the structure. In the first the translational vectors of the unit cell are used to superimpose all of the unit cells of the twenty configurations onto one. In this type of analysis all local information is lost, and one is only able to examine the average atom density. The

mean coordinates of the 8 oxygen and 24 hydrogen sites in the unit cell were calculated in this manner. (This is not altogether appropriate as it assumes a symmetric distribution of displacements, but no better method is possible without making unproven assumptions.) From here inter-site distances and angles were calculated, and their mean values are given in table 1, the notation for which is explained in figure 6. If required, mean square displacements can be obtained by considering the distances of the atoms from these sites.

Table 1. Columns 2–4 give the results of the calculations in which oxygen and deuterium atoms could both move. The second column gives the mean inter-site distances and angles. Columns 3 and 4 relate to the actual bond length and bond angle distributions. The final column gives the mean actual values from the calculation in which the oxygen atoms were fixed to their sites. All distances are in Å, and all angles in degrees. The bracketed figures give standard deviations, as defined in the text.

	Inter-site	Actual		Fixed oxygen
	mean	Mean	FWHM	mean (actual)
O–O″	2.758(4)	2.768(2)	0.36	2.753 (fixed)
O–O′	2.733(3)	2.743(5)	0.36	2.746 (fixed)
O–D_2	0.978(6)	0.999(2)	0.35	0.997(1)
O–D_1	0.970(2)	0.987(4)	0.35	0.999(5)
O- -D_2''	1.780(6)	1.801(3)	0.35	1.794(2)
O- -D_1'	1.763(3)	1.787(6)	0.35	1.785(4)
D_2–D_3	1.593(6)	1.577(6)	0.34	1.579(6)
D_2–D_1	1.594(4)	1.579(5)	0.34	1.581(5)
D_2- -D_3''	2.296(5)	2.318(1)	0.32	2.328(2)
D_2- -D_1'	2.291(6)	2.313(1)	0.32	2.321(2)
O″–O–O″	109.3(1)	109.1(1)	11	109.5 (fixed)
O′–O–O″	109.7(2)	109.5(1)	11	109.5 (fixed)
D_2–O–D_3	109.1(6)	105.6(4)	30	105.1(4)
D_2–O–D_1	109.8(6)	106.1(5)	30	105.1(7)
O–D_2- -O″	179.3(3)	164.3(3)	23	163.0(3)
O–D_1- -O′	179.3(2)	164.4(5)	23	163.2(5)

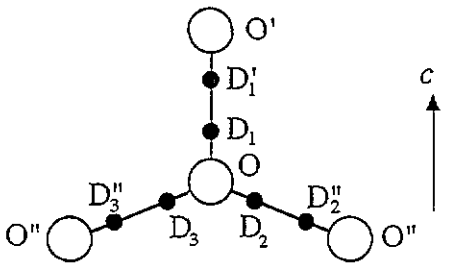

Figure 6. An illustration of the notation used in the text and tables for the various inter-atomic distances and angles.

Instead of using the site positions, it is possible to extract information directly from the configurations themselves. This allows the actual distribution of bond lengths or angles to

be obtained. The mean values obtained in this way will be identical to the mean inter-site values only if there is no static disorder on a local scale. Mean and full-width half-maximum (FWHM) values for the actual bond length and angle distributions are given in table 1, and will be discussed further in the next section.

In table 1 the bracketed figures give the standard deviation, defined for quantity x, with mean value X by

$$\sqrt{\frac{1}{(n-1)}\sum_{i=1}^{n}|x_i - X|^2}. \tag{3}$$

For the inter-site quantities the sum is over all occurrences of that quantity in the eight-molecule unit cell. For the mean of the actual bond lengths and bond angles the x are the mean values from each of the 20 configurations, with X the overall mean. The sizes of the standard deviations in the latter case show that the results of all the independent configurations are in good agreement with one another.

5. Results and discussion

The modelling of single-crystal diffuse scattering in the unconstrained manner described here is a very brave undertaking, and is obviously liable to run into difficulties. Table 1 contains both the mean inter-site distances and angles, and information about the actual bond length and bond angle distributions. In the following these quantities will be discussed and further results presented, with explicit mention of the limitations of the present RMCX technique where appropriate.

All RMC methods produce configurations of atoms which are among the most disordered consistent with the data used in fitting, and this is exacerbated in RMCX because no Bragg scattering is modelled. This leads to mean square displacements being increased over their real values, and to the broadening of bond length and angle distributions. However, for symmetric distributions the increase in FWHM values does not affect the mean. Any correlations present in the model are likely to be in the real material (correlations are not formed by a random increase in disorder); indeed in the real material the correlations are likely to be stronger.

The broadening of the distributions is immediately apparent in table 1, where the FWHM values of the distributions are unrealistically large. This is particularly true for the O–O distribution, where the FWHM is nearly an order of magnitude greater than from spectroscopic techniques. This is because the diffuse scattering from ice is dominated by the contribution from the Bernal–Fowler rules, and hence the O–O contribution to the diffuse scattering is far smaller than the O–D or D–D contributions.

To study the opposite extreme, in which the O–O distribution is kept as narrow as possible, RMCX was run with the oxygens fixed on their sites throughout. This is obviously an unrealistic situation, with the deuteron disorder now having to account for all of the diffuse scattering, which will lead to an increase in the deuteron mean square displacements. The last column of table 1 gives the mean values of the distributions obtained in this way. The results from this calculation are in good agreement with those obtained from the RMCX calculations in which both atomic species were free to move. The biggest change is in the mean O–D distances, which are now approximately the same whether parallel or oblique to the c-axis. This is believed to be because the O–O–O angles are no longer free to change. There are small changes in other quantities. The change in the O–D- -O angle is discussed in section 5.3.

5.1. Effect of the c/a ratio

For perfect tetrahedral coordination, with all O–O–O angles 109.47° and all O–O nearest neighbour distances equal, geometrical considerations require the ratio of the c to a lattice parameters to be 1.633. However, in accurate experimental work Röttger *et al* (1994) find that the c/a ratio is close to 1.628 at all temperatures. This requires either O′–O–O″ (which includes c) to be smaller then O″–O–O″, or the nearest neighbour distance along c, O–O′, to be smaller than O–O″. The crystallographic work of Kuhs and Lehmann (1986) found that the angles were changed, with O′–O–O″ = 109.30(1)° and O″–O–O″ = 109.64(1)° at 60 K, and the bond lengths independent of their orientation.

As table 1 shows, in the present work the angle was found to change in the opposite way, with O′–O–O″ slightly greater than O″–O–O″, compensated by a change in the nearest-neighbour O–O distances, with O–O′ significantly less than O–O″. This may be because the diffuse scattering is largely due to deuteron–deuteron correlations and hence does not contain sufficient information on oxygen–oxygen pair and triplet correlation functions. The O–O distribution is quite symmetric and so the shift is unlikely to be due solely to the enlarged FWHM of this distribution. However, an interesting difference in the RMCX results was found when different high-Q regions of scattering were removed from the data modelled. Three additional models were run to investigate this:

(a) the section of the 0 k l plane with both $k > 4$ and $l > 7$ was removed, as well as the equivalent section in the h h l plane;

(b) the section of the 0 k l plane with both $k < 4$ and $l > 7$ was removed, as well as the equivalent section in the h h l plane;

(c) the section of the h 0 l plane with both $h > 2.4$ and $l > 7$ was removed, as well as the equivalent section in the h $3h$ l plane.

Some of the results of these simulations are given in table 2, and they indicate that when the strong scattering at the highest Q is removed from the 0 k l plane—case (a) above—the difference between O–O′ and O–O″ is largely removed, and the two angles equalized. However, in the calculation in which the oxygen atoms were not free to move a satisfactory fit to the high-Q region of the 0 k l plane was still achieved. Hence the scattering in this region of reciprocal space can be modelled in many ways, and the differences in table 1 between distances and angles oblique and parallel to the c-axis may not be correct. Further data, such as the Bragg peak information or diffuse scattering from other regions of reciprocal space, are necessary to clarify the situation.

Table 2. Mean actual bond lengths and bond angles obtained from fits with different regions of the high-Q scattering removed, as explained in the text. All distances are in Å. The bracketed figures give standard deviations.

	All data fitted	Case (a)	Case (b)	Case (c)
O–O″	2.768(2)	2.764(1)	2.770(2)	2.768(2)
O–O′	2.743(5)	2.757(3)	2.738(5)	2.743(5)
O″–O–O″	109.1(1)	109.3(1)	109.0(1)	109.1(1)
O′–O–O″	109.5(1)	109.3(1)	109.6(1)	109.5(1)

The size of the O–O–O angle is found in all models in which the oxygens were free to move to depend on where the deuterons are placed with respect to the central oxygen. For example O′–O–O″ is 109.9(2)° with two deuterons included near the central oxygen,

109.5(1)° with one deuteron there and only 109.1(2)° when there are no deuterons included near it.

5.2. The molecular shape

The mean value of the actual O–D distribution in our study is 0.996(3) Å, and the mode 0.998 Å. The mean inter-site O–D distance of 0.976(3) Å is significantly lower than the mean value of the distribution.

An isolated water molecule in the ground vibrational state has an O–D distance of 0.9686 Å and angle of 104.57° (Whalley 1974). In ice Ih there has long been debate over the O–D distance, with values close to 1.00 Å obtained from Bragg peak analysis using a half-hydrogen model and the harmonic approximation (Kuhs and Lehmann 1986), compared to a predicted inter-site value close to that for ice II and ice IX (Whalley 1974), i.e. about 0.98 Å (Londono 1989, La Placa *et al* 1973). By using spectroscopic information to take account of local disorder Kuhs and Lehmann (1987) deduced that the inter-site O–D distance had the value of 0.974(7) Å, close to the predicted value. This is in excellent agreement with the value of 0.976(3) Å found in the present study. Local disorder, particularly of the oxygens, also explains why in the present study the mean O–D distance obtained direct from the configurations is larger than the mean inter-site distance. In the latter case the effects of local order cancel, whereas in the former the displacement of the oxygen from its site in a direction away from the deuterons of the same molecule (as discussed in section 5.4) increases the O–D distance.

To illustrate the limitations of RMCX discussed earlier let us consider the RMCX O–D distribution. This is close to Gaussian and so the mean values are reasonably accurate, but it has a FWHM of 0.35 Å. The vibrational mean square displacement along the O–D bond direction is close to 0.0039 $Å^2$ at all temperatures (Kuhs and Lehmann (1986), based on the work of Iogansen and Rozenberg (1978)), which would lead to a FWHM for the O–D distribution of ~0.15 Å, less than half the value obtained from RMCX. Constraints were added to the model to try and decrease the O–D distribution width, but were largely unsuccessful and did not reproduce the data in a sensible manner (see Nield 1995).

The distribution of intra-molecular water angles is very broad but is reasonable considering the size of the librational mean square displacement (see Kuhs and Lehmann 1986). The mean is 105.8(5)°. The mean inter-site angle is close to tetrahedral, as required by symmetry. The water molecule angle in ice is therefore increased over the free molecule value, but does not attain the tetrahedral angle. The values found for several phases of ice agree well with the 105.8(5)° found here, for example 107(1)° for ice Ih (Kuhs and Lehmann 1987), 106(1)° for ice IX (La Placa *et al* 1973, Londono *et al* 1993), 106.0(4)° for ice II (Londono 1989) and 106(1)° for the high pressure ice VIII (Kuhs *et al* 1984).

5.3. Hydrogen bond configuration

Once it is accepted that the D–O–D angle is significantly different from the O–O–O angle it is clear that the O–D- -O angle must differ from 180°. The minimum such deviation, of close to 3°, would be achieved if the water molecule lies symmetrically within the O–O–O angle. The present results indicate that in ice Ih the O–D- -O angle actually has a mean value of 164.3°, and a mode which is slightly higher than this, at about 168°. Figure 7 shows the angle distribution for O–D- -O. Its shape can be explained by realizing that the solid angle available to the O–D bond is small when the angle is close to 180°. Hence assuming Gaussian or similar thermal distributions about the sites there will be a maximum

in the angle distribution, caused by the competing effects of increasing solid angle and decreasing deuteron density as one moves from the site.

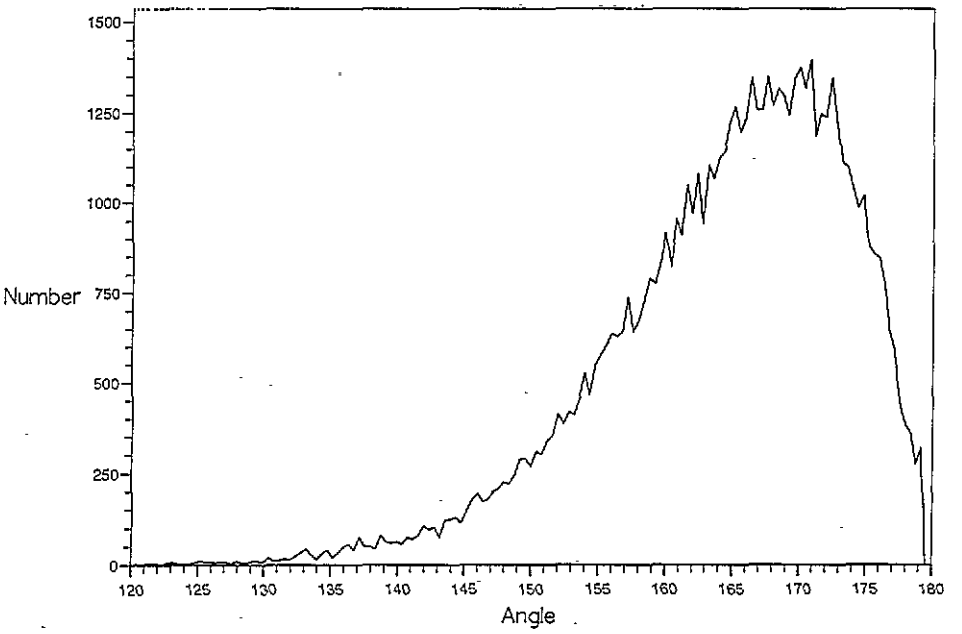

Figure 7. The O–D- -O angle distribution obtained in the RMCX model, with the oxygen atoms not fixed.

The deviation of the mean O–D- -O angle from the straight bond is entirely consistent with the size of the mean square displacements present (in both the model with the oxygen atoms fixed and the one with both atomic species free to move). Hence the true mean O–D–O angle in ice Ih is close to 170° (using the accurate mean square displacements from Kuhs and Lehmann 1987). Within statistics the bond bending occurs with equal probability in all directions perpendicular to the bond.

5.4. Oxygen disorder

As discussed in subsection 5.2 the O–D inter-site values are significantly less than the mean actual O–D values. This can, at least in part, be ascribed to disorder of the oxygen atoms caused by the deuteron disorder. From the RMCX configurations the average displacement of the oxygen atom along the bisectrix of the molecule was calculated, and found to be 0.011(2) Å away from the deuterons of the same molecule. Kuhs and Lehmann's (1986, 1987) interpretation, from Bragg analysis and spectroscopic information, was that the displacement was approximately 0.05(2) Å along the bisectrix. As explained at the start of this section the nature of RMC modelling means that correlations such as this are likely to be decreased, which is consistent with the above.

It was investigated whether a molecule tends to move in the same or the opposite direction to its four surrounding molecules. The average direction of displacement of the oxygen atoms of these surrounding molecules was calculated, and the component of the displacement of the central oxygen along this direction determined. The average such displacement was 0.025(4) Å in the direction of the surrounding oxygens. Hence the molecules tend to move with rather than against their four neighbours.

6. The strong scattering along 6 0 *l*

In section 2 it was mentioned that the main differences between experiment and the Bernal–Fowler simulation were the patch of scattering at high Q in the 0 k l plane and the streak of scattering along 6 0 l. This latter feature was ascribed by Schneider and Zeyen (1980) to additional one-dimensional disorder, such as stacking faults. Stacking faults are unlikely to be present in quantities large enough to cause a signature of this magnitude, as explained in Li *et al* (1994). Moreover if they were present disorder would be generated in the orthorhombic b-direction, leading to strong scattering along 0 2 l, 0 4 l and so on (in our orthorhombic notation). Such additional features were not seen in the experimental 0 k l data. Hence explanation of the strong scattering along 6 0 l lies elsewhere.

Using the RMCX obtained configuration the scattering due solely to the deuterons was calculated, and found to account for more than 70% of the intensity of the 6 0 l streak. Theoretically streaks along 2 0 l, 4 0 l, 6 0 l and so on can be produced by having different layers perpendicular to the c-axis displaced from their initial positions along the a-direction in a random manner, so that atoms in adjacent layers are not lined up along c. In ice the streak along 6 0 l is particularly strong compared to the streaks along 2 0 l and 4 0 l because the deuterium–deuterium separations along this direction are close to 1/6 of the a lattice parameter.

The streak can be reproduced in simulation by starting from the configuration obtained from the initial Bernal–Fowler model, and then moving all deuterons in the same layer (defined either as all deuterons in the same plane perpendicular to c, or as all deuterons in molecules with oxygen atoms in such a plane) by Δ, 0 or $-\Delta$ from their sites along the a-direction, with the specific displacements chosen at random for each layer. Slightly different definitions of 'layer' cannot be differentiated between, provided the layer is perpendicular to the c-axis. Similarly the size of Δ is ill defined, but displacements of order 0.05 Å are certainly sufficient. If the oxygen atoms are moved with the deuterons the streak is further reinforced, and a smaller Δ is necessary. The above has not considered the symmetry of ice, and in particular the planes corresponding to h 0 l. Considering these there are six equivalent streaks, which can be produced in a way which preserves symmetry by moving molecules in a plane perpendicular to c by either Δ, 0 or $-\Delta$ along any of the directions equivalent to a.

Hence the diffuse scattering clearly indicates that in ice Ih deuterons, or more probably complete molecules, which are in planes perpendicular to the c-axis move together along specific directions. The resolution of the measurement is not good enough to determine exactly how many molecules move in a coherent manner, but, from the width of the measured streak, it is probably of the order of ten. The molecules in adjacent planes move in different directions.

7. Conclusions

A novel reverse Monte Carlo technique has been used to model single-crystal neutron diffuse scattering from D_2O ice Ih. Although this technique has limitations at present it in principle allows more information to be obtained from the diffuse scattering of ice than was achievable previously. Much of this information cannot be accessed using standard Bragg analysis techniques. To allow the validity of the model results to be examined a second reverse Monte Carlo model was obtained, in which the oxygen atoms were fixed on their sites.

In both cases it was found that the water molecule in ice Ih has an angle significantly

smaller than tetrahedral, but larger than the free molecule value. The actual O–D distance is close to 1.0 Å, this large value being caused by local disorder in the system, such as the displacement of the oxygen along the bisectrix of the molecule away from the deuterons of that molecule. On calculating the mean site coordinates, so that all local information is lost, the O–D distance was between 0.02 and 0.03 Å smaller. The average O–D- -O angle deviates considerably from 180° mostly because of the large librational motion of the deuteron.

The most unexpected finding of this study is that, over many unit cells, the molecules in planes perpendicular to the *c*-axis move together along the orthorhombic [100] or its equivalent directions. This conclusion does not depend on modelling, and has important implications for other properties of ice Ih.

Acknowledgments

SERC research grants which supported one of us (VMN) and provided the workstation used in this study are gratefully acknowledged. Many thanks go to J-C Li, who measured the experimental data used in this study, and to J W Glen, D A Keen, W F Kuhs and D K Ross for helpful discussions.

References

Bernal J D and Fowler R H 1933 *J. Chem. Phys.* **1** 515
Bragg W H 1922 *Proc. Phys. Soc.* **34** 98
Descamps M and Coulon C 1977 *Chem. Phys.* **25** 117
Goto A, Satoh K, Hondoh T and Mae S 1992 *Physics and Chemistry of Ice* ed N Maeno and T Hondoh (Sapporo: Hokkaido University Press) p 69
Iogansen A V and Rozenberg M Sh 1978 *Opt. Spektrosk.* **44** 87
Kamb B 1973 *Physics and Chemistry of Ice* ed E Whalley, S J Jones and L W Gold (Ottawa: Royal Society of Canada) p 39
Kuhs W F, Finney J L, Vettier C and Bliss D V 1984 *J. Chem. Phys.* **81** 3612
Kuhs W F and Lehmann M S 1986 *Water Sci. Rev.* **2** 1
——1987 *J. Physique Coll.* **48** C1 3
La Placa S J, Hamilton W C, Kamb B and Prakash A 1973 *J. Chem. Phys.* **58** 567
Li J-C, Nield V M, Ross D K, Whitworth R W, Wilson C C and Keen D A 1994 *Phil. Mag.* B **69** 1173
Londono J D 1989 *PhD Thesis* University of London
Londono J D, Kuhs W F and Finney J L 1993 *J. Chem Phys.* **98** 4878
McGreevy R L and Howe M A 1992 *Annu. Rev. Mater. Sci.* **22** 217
McGreevy R L and Pusztai L 1988 *Mol. Simul.* **1** 359
Metropolis N, Rosenbluth A W, Rosenbluth M N, Teller A H and Teller E J 1953 *J. Chem. Phys.* **21** 1087
Nield V M 1995 *Nucl. Instrum. Methods* A **354** 30
Nield V M, Keen D A and McGreevy R L 1995 *Acta Crystallogr.* A at press
Owston P G 1949 *Acta Crystallogr.* **2** 222
Peterson S W and Levy H 1957 *Acta Crystallogr.* **10** 70
Röttger K, Endriss A, Ihringer J, Doyle S and Kuhs W F 1994 *Acta Crystallogr.* B **50** 644
Schneider J 1975 *Thesis* Technische Universität München
Schneider J and Just W 1975 *J. Appl. Crystallogr.* **8** 128
Schneider J and Zeyen C 1980 *J. Phys. C: Solid State Phys.* **13** 4121
Villain J and Schneider J 1973 *Physics and Chemistry of Ice* ed E Whalley, S J Jones and L W Gold (Ottawa: Royal Society of Canada) p 285
Whalley E 1974 *Mol. Phys.* **28** 1105